

FitDiff: Robust monocular 3D facial shape and reflectance estimation using Diffusion Models

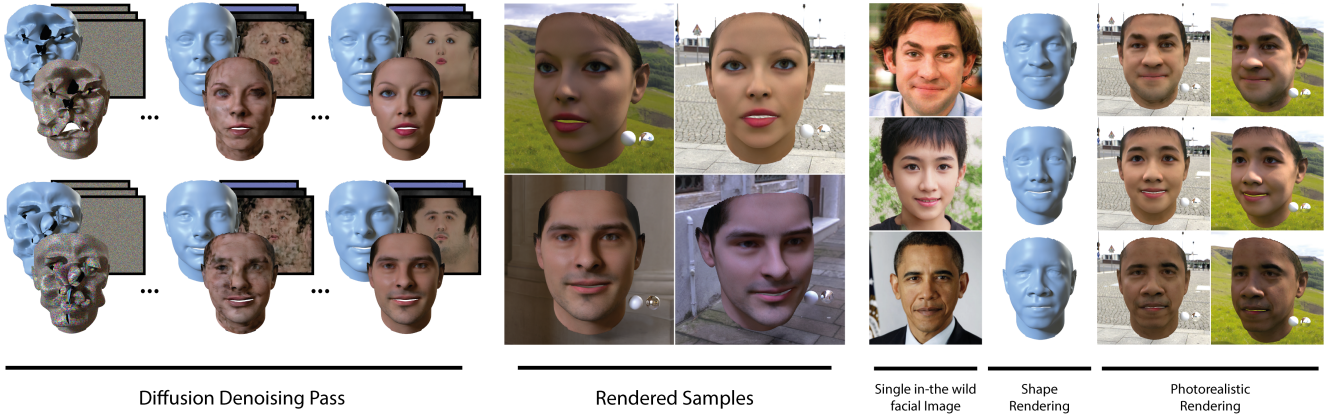
Stathis Galanakis^{1,2}Alexandros Lattas^{1,2}Stylianos Moschoglou²Stefanos Zafeiriou¹¹Imperial College London²Huawei UK

Figure 1. FitDiff is a multi-modal diffusion model conditioned on facial identity embeddings, that generates facial shape and reflectance, from a single “in the wild” facial image. Our method reconstructs facial avatars which then can be photorealistically rendered as-is.

Abstract

The remarkable progress in 3D face reconstruction has resulted in high-detail and photorealistic facial representations. Recently, Diffusion Models have revolutionized the capabilities of generative methods by achieving far better performance than GANs. In this work, we present FitDiff, a diffusion-based 3D facial avatar generative model. This model accurately generates relightable facial avatars, utilizing an identity embedding extracted from an “in-the-wild” 2D facial image. Our multi-modal diffusion model concurrently outputs facial reflectance maps (diffuse and specular albedo and normals) and shapes, showcasing great generalization capabilities. It is solely trained on an annotated subset of a public facial dataset, paired with 3D reconstructions. We revisit the typical 3D facial fitting approach by guiding a reverse diffusion process using perceptual and face recognition losses. Being the first LDM conditioned on face recognition embeddings, FitDiff reconstructs relightable human avatars, that can be used as-is in common rendering engines, starting only from an unconstrained facial image, and achieving state-of-the-art performance. Project website: stathisgl.github.io/fitdiff/

1. Introduction

A fundamental objective of the field of Computer Vision encompasses the photorealistic 3D face reconstruction from a single image and has gained significant attention from the research community over the past few decades. Its numerous applications in computer graphics, virtual reality, and entertainment, include avatar creation, face manipulation, and face animation [3, 24, 41, 53]. Despite the notable recent progress, accurate replication of personalized facial reconstructions continues to present a challenge. This is primarily due to the inherent ambiguity present in monocular images, as well as the difficulties associated with handling occlusions and capturing substantial variations in lighting conditions and facial expressions. On top of that, 3D facial datasets are still relatively small [103], including biases and lacking generalization in parallel with structural limitations of the current facial reconstruction methods.

The 3D Morphable Model (3DMM) was introduced in the seminal work of Blanz and Vetter [6] and uses Principal Component Analysis (PCA) to model the complex facial shapes and textures of 200 facial scans. Since then, there has been tremendous progress in retrieving 3D facial information from a monocular image like large-scale sta-

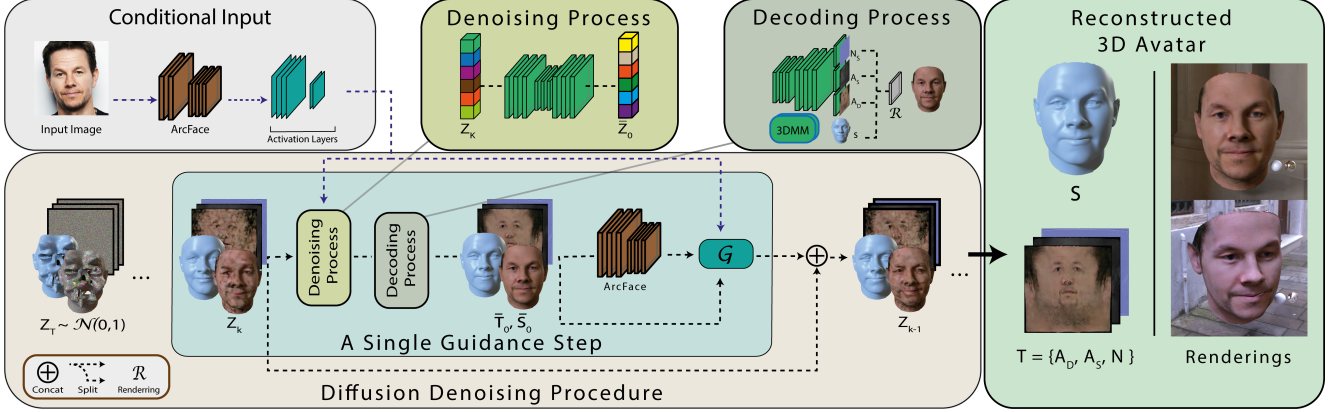


Figure 2. Overview of FitDiff, a latent diffusion-based 3D facial generative network. Starting from Gaussian noise, our method generates facial avatars with relightable reflectance and shape, conditioned on an identity embedding. During sampling, a novel guidance algorithm is applied for further control of the resulting identity. Z_T , Z_k and Z_{k-1} are visualized in the actual picture space for illustration purposes.

tistical models utilizing hundreds of subjects [9, 46, 63]. Even though most statistical models can accurately reconstruct the facial shape, they do not perform well in capturing the facial texture [9]. More recently, Generative Adversarial Networks (GANs) [30], and particularly the style-based generators [36–38], have demonstrated effectiveness in capturing intricate frequencies. This success has resulted in numerous subsequent studies combining these methods with 3DMMs [24, 26, 27], where the facial texture is modeled as a UV map. Those methods include a fitting phase that involves optimizing a loss function. Additionally, some approaches generate high-fidelity facial reconstructions via implicit representations [14, 22, 23, 33, 58, 102], while others focus on relightable facial reconstructions [41, 42, 83]. A fundamental challenge inherent in optimization fitting methods is their susceptibility to outliers [44]. Furthermore, despite the remarkable performance achieved by GAN-based generative facial models, they still suffer from problems like unstable training and mode collapse [40, 73].

A solution to the aforementioned problems is the integration of the recent emerging Diffusion Models (DMs) [32]. These architectures have gained a lot of attention lately because of their current state-of-the-art performance in image synthesis tasks [17]. Taking inspiration from the thermodynamics [78], DMs define a T -length Markov Chain by gradually adding normally distributed random noise to the data and learn to predict the input noise for each step $t \in \{1, 2, \dots, T\}$. They synthesize new data by reversing the diffusion process, starting from a normally distributed random noise and progressively denoising it. A family of those networks is the Latent Diffusion methods [71, 89], which operate the diffusion process in the latent space instead of the pixel space directly. Their applications include medical tasks [64], text-to-audio approaches [48] and video

creation [7]. These robust methods have been proven to perform on par with pixel space diffusion approaches [89] whilst getting trained faster [71]. Lately, a large number of text-input diffusion-based techniques have emerged for the synthesis of facial images [91, 99]. Rodin [91] uses diffusion models to generate avatars using an implicit representation, and DreamFace [99] generates relightable facial assets from text input. However the first is slow and not compatible with standard rendering, while the latter cannot be used for single-image reconstruction. Nevertheless, it is noteworthy to emphasize that most of the aforementioned methods employ a conditional mechanism reliant on textual descriptions or other auxiliary information [66], thereby directing their attention not exclusively towards the faithful reconstruction of facial identity and the exploration of the potential of robust identity embeddings.

This study presents FitDiff, a multi-modal generative model, based on latent diffusion. By harnessing the impressive generation capabilities of LDMs [71], we delve into their potential in the field of 3D facial reconstruction. Our approach enables the synthesis of facial avatars by combining facial UV reflectance maps and facial geometry while utilizing an identity embedding layer as a conditioning mechanism. The diffusion process is applied to the concatenation of the latent vectors of the facial texture maps and shape, while a VQGAN AutoEncoder [19] and a 3DMM model (LSFM [9]) are used to decode them. Moreover, we present a novel facial guidance algorithm incorporated into the reverse diffusion process for accurately reconstructing a target facial identity. FitDiff generates high-fidelity facial avatars while achieving a state-of-the-art identity preservation score. The training of our model involves fitting a facial reconstruction network [43] to a manually selected set of images acquired from the CelebA-HQ dataset [35]. The

fitting process results in acquiring facial shape and facial reflectance maps. Overall, in this paper:

- We introduce FitDiff, a multi-modal diffusion-based generative model that jointly produces facial geometry and appearance. The facial appearance consists of facial diffuse albedo, specular albedo, and normal maps, enabling photorealistic rendering.
- We show the first diffusion model conditioned on identity embeddings, acquired from an off-the-shelf face recognition network, whilst introducing a SPADE [61]-conditioned UNet architecture.
- We present unconditional samples of relightable avatars, but most importantly, we achieve facial reconstruction from a single “in-the-wild” image through identity embedding conditioning and guidance.

2. Related Work

2.1. Face Modeling

A wide variety of works followed the introduction of the emblematic first 3D Morphable Model (3DMM) [6] trained on 200 distinct subjects. Numerous works have since proposed improvements, especially on realistic expressions [2, 10, 11, 13, 45, 46, 86, 95], large-scale dataset and model releases [8, 15, 63, 77]. However, those models were unable to capture high-frequency details due to their linear nature. To deal with this, many studies integrated 3DMMs with Deep Neural Networks [84, 88], Mesh Convolutions [56], GANs [24, 25, 27] and VAEs [4, 50, 68, 92]. Lately, several works focus on acquiring either facial shape [21, 93, 103] or reflectance texture maps, [41, 42]. Some other approaches [18, 43, 51] concurrently reconstruct both while requiring separate models for geometry and appearance. Moreover, the photorealistic rendering of implicit representation-based methods [54, 60] led to numerous approaches [3, 22, 23, 33, 53, 58, 97]. However, their applications and editability remain challenging, hence this work focuses on explicit representations. For a more comprehensive exploration of the methodologies employed in 3D face modeling, we refer the reader to [75].

2.2. Diffusion Models

Inspired by [78, 80–82], the authors of [17] showed that DMs can perform better than the widely used GAN-based methods in image synthesis tasks. DMs learn to model a data distribution $\mathcal{P}(x)$ by gradually injecting normally distributed noise as a T -length Markov Chain and predicting the denoised data in each step. The reverse denoising process can be used as the sampling procedure. The high-quality samples and the more stable training have attracted the attention of the research community leading to a great variety of applications in image generation [31, 67, 71], text-to-image [39, 57], text-to-3D [65],

Pointcloud [52, 98, 101] and Mesh [49] generation. One significant limitation of DMs is their sampling speed, which is hindered by their iterative generative nature. Despite the introduction of DDIMs [79], which helped decrease sampling time, a significant amount of computational resources is still necessary for each iteration step. Initial approaches like [76, 89] and then Latent Diffusion Models (LDMs) [71] perform the diffusion process in the latent space, instead of the pixel space, while achieving comparable performance in image synthesis. Extensions of those methods broaden the applications into medicine [64], text-to-audio [48], and video creation [7]. On top of that, some approaches [47, 94] use a pre-trained LDM as priors. Closest to our work, two other diffusion-based facial models [91, 99] were presented. Both of them employ a coarse-to-fine approach to attain precise identity details, in contrast to our single-stage methodology. Furthermore, Rodin [91] uses an implicit representation [14] for facial shape, while our approach integrates a fully-controllable 3DMM model.

3. Method

In this work, we propose FitDiff, a latent-diffusion-based approach to reconstruct facial avatars. We harness the power of diffusion models for the generative and fitting process as, by nature, they are very robust in both processes since they directly operate on the image space [71]. On the other hand, GANs suffer from various issues such as mode collapse during training [85] or unrealistic outputs in fitting methods, resulting in unnecessary heuristics [43] to stabilize the outputs at the expense of fidelity.

A facial avatar can be formulated as a combination of a mesh \mathbf{S} , and texture \mathbf{T} which is defined as a combination of facial reflectance UV maps, namely diffuse albedo (\mathbf{A}_D), specular albedo (\mathbf{A}_S) and normals (\mathbf{N}). Also, let us denote an “in-the-wild” image containing a face as \mathbf{I} , and \mathbf{V}_{tgt} as the corresponding target identity embedding of the appearing face. Given \mathbf{V}_{tgt} as input, FitDiff generates a 3D facial avatar of the same identity as the one in \mathbf{I} alongside with current scene’s illumination parameters (ambient, diffuse, and specular lighting and lighting direction). An overview of our method is illustrated in Fig. 2, whereas the rest of the section includes a detailed presentation of our method’s architecture (Sec. 3.1), the proposed conditional input (Sec. 3.2), the training scheme (Sec. 3.3), and finally the identity-guidance sampling procedure (Sec. 3.4).

3.1. Model Architecture

FitDiff is a latent-diffusion based approach [71]. This is motivated by the challenges posed by the large number of parameters and the computational expenses associated with generating multiple meshes and texture images simultaneously. Thus, we represent facial avatars as a latent vector containing latent information about the shape, facial tex-

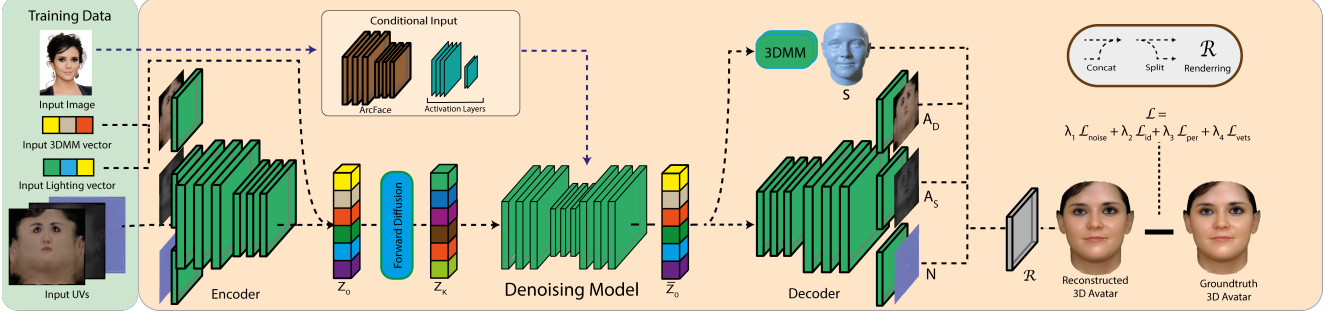


Figure 3. Overview of the main phase of our training scheme: During each training iteration, the facial reflectance maps are initially projected onto the latent space and subsequently concatenated to the latent vector \mathbf{z}_0 , to which noise is introduced. Following the estimation of the initial $\bar{\mathbf{z}}_0$, perceptual and face recognition losses are imposed upon the estimated initial avatar.

ture, and scene illumination: $\mathbf{z} = \{\mathbf{z}_{tex} | \mathbf{z}_{shp} | \mathbf{z}_{ill}\} \in \mathbb{R}^{4288}$, where $\mathbf{z}_{tex} \in \mathbb{R}^{4096}$ signifies the facial reflectance latent vector, $\mathbf{z}_{shp} \in \mathbb{R}^{183}$ the latent shape vector and $\mathbf{z}_{ill} \in \mathbb{R}^9$ the scene illumination parameters. The latent shape vector \mathbf{z}_{shp} can be further separated into the identity parameters $\mathbf{z}_{shp_i} \in \mathbb{R}^{158}$ and expression parameters $\mathbf{z}_{shp_e} \in \mathbb{R}^{25}$.

FitDiff is composed of a 3D statistical model \mathcal{F}_{shp} (LSFM [9]) that generates facial geometry, a branched multi-modal AutoEncoder [19, 71] that generates facial reflectance maps, and a denoising UNet AutoEncoder [72]. For a set of identity \mathbf{z}_{shp_i} and expression \mathbf{z}_{shp_e} parameters, the PCA face model \mathcal{F}_{shp} generates a facial mesh \mathbf{S} following the formula:

$$\mathbf{S} = \mathcal{F}_{shp}(\mathbf{z}_{shp}) = \mathbf{U}_i \cdot \mathbf{z}_{shp_i} + \mathbf{U}_e \cdot \mathbf{z}_{shp_e} + \mathbf{m}_i$$

where \mathbf{U}_i and \mathbf{U}_e are the identity and expression bases, respectively, and \mathbf{m}_s is the mean face. Additionally, we incorporate a robust branched VQGAN [19, 71], to function as a multi-modal texture UV generator. More specifically, the VQGAN encoder \mathcal{E} concurrently encodes facial diffuse albedo \mathbf{A}_D , specular albedo \mathbf{A}_S and normals \mathbf{N} into the same latent vector \mathbf{z}_{tex} , whereas the VQGAN decoder \mathcal{D} reconstructs them given the input latent vector \mathbf{z}_{tex} . Finally, following common diffusion-based methods [17, 32, 71], we utilize a UNet AutoEncoder [72] with self-attention [90] layers $e_\theta(x_t, t)$ conditioned to the input time step $t \in \{1, \dots, T\}$. We train the UNet to predict the injected noise ϵ , sampled from a standard normal distribution, i.e., $\epsilon \sim \mathcal{N}(\mathbf{0}, \mathbf{1})$. The training details of our method are presented in Sec. 3.3.

3.2. Conditional input

In the underlying UNet model, we integrate a powerful conditioning mechanism to effectively learn all the necessary identity information. An ideal identity embedding must contain both low and high-frequency information aiming to accurately reconstruct the desired facial avatar. To acquire

such an identity embedding, we employ a powerful identity recognition network [16], to which we feed the input facial image. Then, the resulting conditioning vector is a combination of the last feature vector with the intermediate activation layers of the identity recognition network.

Let \mathcal{C}^n be the n -th intermediate layer of the identity recognition network. We extract the intermediate activation maps $\mathcal{C}^2 \in \mathbb{R}^{128 \times 28 \times 28}$, $\mathcal{C}^3 \in \mathbb{R}^{256 \times 14 \times 14}$, $\mathcal{C}^4 \in \mathbb{R}^{512 \times 7 \times 7}$ and concatenate them channel-wise with the identity embedding $\mathbf{V} \in \mathbb{R}^{512}$, which is expanded spatially. Because of the 2D nature of our identity embedding and following [22], we use SPADE layers [61] as a conditioning mechanism to inject \mathbf{V} into the intermediate layers of the UNet.

3.3. Model Training

Our training scheme consists of two phases: Initially, we conduct the training for the branched texture AE, followed by the subsequent training for the denoising UNet model. The first part of our training protocol entails the training of the branched multi-modal AE [19], whereby triplets are employed as input data:

$$x = \{\mathbf{A}_D, \mathbf{A}_S, \mathbf{N}\}, \quad \mathbf{A}_D, \mathbf{A}_S, \mathbf{N} \in \mathbb{R}^{512 \times 512 \times 3}$$

where \mathbf{A}_D represents the diffuse albedo, \mathbf{A}_S the specular albedo and \mathbf{N} the normals. Our approach includes a branched multi-modal discriminator [43] in combination with a perceptual loss [100] as the training loss. The discriminator is a path-based discriminator [19] comprising two branches, to accommodate their different statistics [43]. The first branch gets as input the concatenation of diffuse and specular albedos $\mathbf{A}_D \oplus \mathbf{A}_S$, whereas the second branch receives the normals \mathbf{N} . Furthermore, we adhere to the default training parameters outlined in [71]. For a given triplet x_k , the encoder \mathcal{E} projects x_k into a latent representation $\mathbf{z}_{tex} = \mathcal{E}(x_k)$, where $\mathbf{z}_{tex} \in \mathbb{R}^{h \times w \times c}$. Then, the latent vector \mathbf{z}_{tex} is fed into the decoder \mathcal{D} , which produces a reconstructed output triplet \bar{x}_k . We downsample the in-

put texture UVs by a factor of $f = H/h = 512/64 = 8$, following the downsampling investigations in [71] and due to computational limitations. For the shape decoder, we use an LSFM [9] model, pre-trained in $\sim 10k$ identities.

After training the texture AutoEncoder, we freeze its weight parameters and embark on the training of the identity-conditioned UNet. A comprehensive overview of this training approach is presented in Fig. 3. During this phase, we employ multiple components including the identity embedding \mathbf{V}_{tgt} , the shape \mathbf{z}_{shp} , the distinct facial texture maps \mathbf{A}_D , \mathbf{A}_S , and \mathbf{N} , and the scene lighting \mathbf{z}_{ill} . At each training step, the facial reflectance maps undergo an initial encoding by the pre-trained encoder \mathcal{E} , thereby yielding the latent texture vector \mathbf{z}_{tex} . Then, the input vectors are concatenated, i.e., $\mathbf{z}_0 = \{\mathbf{z}_{tex} | \mathbf{z}_{shp} | \mathbf{z}_{ill}\}$. Let us denote \mathbf{z}_t the noisy counterparts of \mathbf{z}_0 , resulting from t steps of noise injection. The UNet network gets \mathbf{z}_t as input, and learns to predict the injected noise following:

$$L_{noise} := \mathbb{E}_{\mathcal{E}(x), \epsilon \sim \mathcal{N}(0,1), t} [\|\epsilon - \epsilon_\theta(\mathbf{z}_t, t, \mathbf{V})\|] \quad (1)$$

where ϵ is the ground-truth injected noise, ϵ_θ the predicted injected noise from \mathbf{z}_t , t the diffusion time step, and \mathbf{V} signifies the 2D identity embedding vector as described in Sec. 3.2.

In addition to the primary loss function \mathcal{L}_{noise} , our training scheme integrates additional losses intended to enhance robustness, which are the identity losses [24, 43] \mathcal{L}_{id} , \mathcal{L}_{per} and the shape loss \mathcal{L}_{verts} . Detailed definitions for those are provided in the supplemental. It is important to note that these auxiliary losses are not applicable to the latent variables. Thus, the estimated initial latent vector $\bar{\mathbf{z}}_0$ is computed as: $\bar{\mathbf{z}}_0 = \frac{\mathbf{z}_t - \sqrt{1-\alpha_t}\epsilon}{\sqrt{\alpha_t}}$. The vector $\bar{\mathbf{z}}_0$ is further decoded into the estimated initial avatar. Firstly, $\bar{\mathbf{z}}_0$ is split into the estimated initial latent texture vector $\bar{\mathbf{z}}_{0tex}$, latent shape vector $\bar{\mathbf{z}}_{0shp}$ and scene parameters $\bar{\mathbf{z}}_{0ill}$. The first two vectors are fed into the decoder \mathcal{D} and the PCA model \mathcal{F}_{shp} respectively. In this way, the estimated initial facial reflectance maps $\bar{\mathbf{T}}_0$ and shape $\bar{\mathbf{S}}_0$ are retrieved. Additionally, under the estimated initial scene illumination $\bar{\mathbf{z}}_{0ill}$, we acquire the initial identity rendering $\bar{\mathbf{I}}_0$ using a differentiable renderer [69], while using a differentiable multi-texture map shader as introduced in [42, 43]. Overall, the conditional denoising model is trained using the following formula:

$$\mathcal{L} = \mathcal{L}_{noise} + \mathcal{L}_{id} + \mathcal{L}_{per} + \mathcal{L}_{verts}$$

where \mathcal{L}_{noise} is defined in Eq. 1, \mathcal{L}_{id} is the identity distance, \mathcal{L}_{per} the identity perceptual loss and \mathcal{L}_{verts} the shape loss.

Even though both the forward and the reversed diffusion processes can be described via stochastic differential equations in a continuous time [82], they can also be applied in discrete time by choosing a very small step, each time. The selection of the appropriate number of diffusion steps

is based on the premise that, in the final step, the input data should be completely converted into random noise. We follow the training parameters proposed by the authors of [71] and we choose $T = 1000$ while using a linear noise schedule. Furthermore, FitDiff is trained following the Classifier-Free approach [31]. This means that, during training, we randomly set the input identity embedding equal to zero with a probability of $\mathcal{P}_{uncond} = 0.1$.

3.4. Sampling Procedure

Algorithm 1 Diffusion sampling using Identity Guidance

Input: A facial “in-the-wild” image \mathbf{I} , a gradient scale s , and networks $\mathcal{C}, \mathcal{M}, \mathcal{F}_{shp}, \mathcal{D}$ as defined in Sec. 3.1, 3.4.

Output: $\mathbf{z}_0 = \{\mathbf{z}_{tex} | \mathbf{z}_{shp} | \mathbf{z}_{ill}\}$ as defined in Sec. 3.1.

- 1: $\mathbf{z}_T = \{\mathbf{z}_{tex_T} | \mathbf{z}_{shp_T} | \mathbf{z}_{ill_T}\} \sim \mathcal{N}(\mathbf{0}, \mathbf{I})$
 - 2: $\mathbf{V}_{tgt} = \mathcal{C}(\mathbf{I})$
 - 3: **for all** t **from** T **to** 1 **do**
 - 4: $\mu, \Sigma \leftarrow \epsilon_\theta(\mathbf{z}_t, t, \mathbf{V}_{tgt})$
 - 5: $\bar{\mathbf{z}}_0 = \frac{\mathbf{z}_t - \sqrt{1-\alpha_t}\epsilon_\theta(\mathbf{z}_t, t, \mathbf{V}_{tgt})}{\sqrt{\alpha_t}}$
 - 6: $\bar{\mathbf{I}}_0 \xleftarrow{\text{render}} \bar{\mathbf{T}}_0, \bar{\mathbf{S}}_0 \xleftarrow[\mathcal{D}, \mathcal{F}_{shp}]{\text{decode}} \bar{\mathbf{z}}_0$
 - 7: $\mathcal{G}_{id}^{cos} \leftarrow (1 - \cos(\mathbf{V}_{tgt}, \mathcal{C}(\bar{\mathbf{I}}_0)))$
 - 8: $\mathcal{G}_{id}^{per} \leftarrow \sum_i \frac{\mathcal{C}^i(\bar{\mathbf{I}}_0) \cdot \mathcal{C}^i(\mathbf{I})}{H_{ci} \cdot W_{ci} \cdot C_{ci}}$
 - 9: $\mathcal{G}_{mse} \leftarrow \|\bar{\mathbf{I}}_0 - \mathbf{I}\|, \mathcal{G}_{lan} \leftarrow \|\mathcal{M}(\bar{\mathbf{I}}_0) - \mathcal{M}(\mathbf{I})\|$
 - 10: $\mathcal{G} = \mathcal{G}_{id}^{cos} + \lambda_1 \cdot \mathcal{G}_{id}^{per} + \lambda_2 \cdot \mathcal{G}_{mse} + \lambda_3 \cdot \mathcal{G}_{lan}$
 - 11: $\mathbf{z}_{t-1} \sim \mathcal{N}(\mu - s\Sigma\nabla_{\mathbf{z}_t}\mathcal{G}, \Sigma)$
 - 12: **end for**
 - 13: **return** \mathbf{z}_0
-

DMs generate new samples by reversing the diffusion process, commencing from an initial random Gaussian noise. In parallel, the authors of [79] introduced Denoising Diffusion Implicit Models (DDIMs) which are implicit probabilistic models [55]. They conduct a modified reverse diffusion process with fewer diffusion steps compared to those required during the vanilla DDPM sampling.

In our method, we adopt the DDIM sampling technique and integrate it into our trained architecture for the generation of facial avatars. We select the number of sampling steps to be $T = 50$ for the DDIM sampling process. Aiming to generate accurate photorealistic avatars, we employ a novel guidance algorithm alongside the conditional input. Our approach is inspired by [17], in which the authors introduce a score corrector network conditioned on the diffusion step. In our implementation, we incorporate a face recognition network \mathcal{C} [16] as a score corrector alongside with an off-the-shelf facial landmark detector \mathcal{M} [12]. The guidance method can be implemented for the vanilla DDPM [17] and the DDIM [79] sampling techniques. For the generation of intermediate images, we employ a differentiable renderer [69] with the modifications introduced

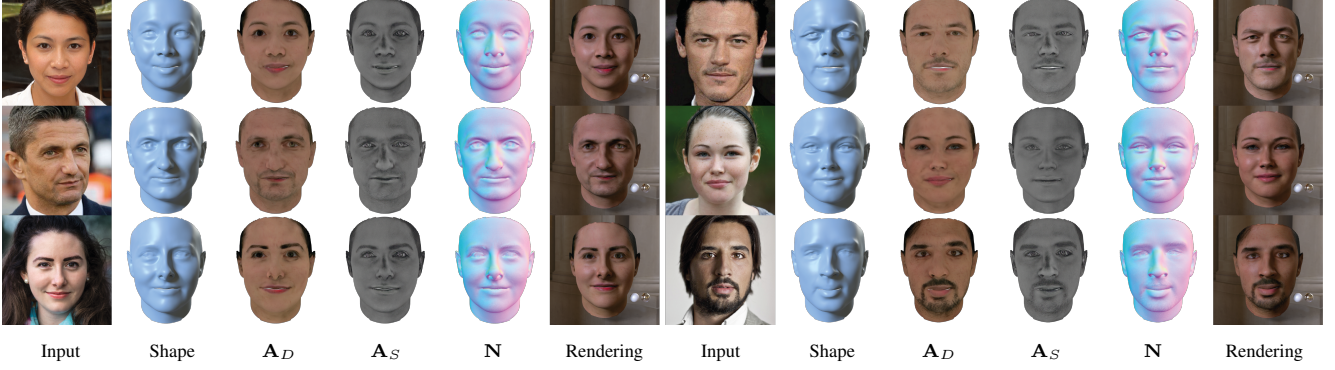


Figure 4. Qualitative results of FitDiff on “in-the-wild” facial images, showing shape, reflectance, and environment map renderings.

in [42, 43]. The pseudo-code of the proposed guidance method is presented in Algorithm 1 while the guidance formula is the following:

$$\mathcal{G} = \mathcal{G}_{id}^{cos} + \lambda_1 \mathcal{G}_{id}^{per} + \lambda_2 \mathcal{G}_{mse} + \lambda_3 \mathcal{G}_{lan} \quad (2)$$

where \mathcal{G}_{id}^{cos} denotes the cosine similarity between the identity vectors, \mathcal{G}_{id}^{per} the identity perceptual similarity, \mathcal{G}_{mse} the photometric loss and \mathcal{G}_{lan} is the distance between the 3D facial landmarks extracted by using \mathcal{M} [12]. Fig. 4 showcases examples of our method being applied to “in-the-wild” images. Following Algorithm 1, we feed the input image \mathbf{I} into \mathcal{C} , to extract the latent identity embedding vector \mathbf{V}_{tgt} and the intermediate activation maps. On top of that, we conduct an alignment step wherein the scene parameters of \mathbf{I} are extracted by using a face detection network [74] and \mathcal{M} . For each reverse diffusion step $t \in \{T, \dots, 1\}$, we firstly predict the expected generated latent parameters, which are decoded. Then, they are rendered and the expected facial image $\bar{\mathbf{I}}_0$ is generated. We compare the identity embedding vectors between the target image \mathbf{I} and the expected facial image $\bar{\mathbf{I}}_0$ by using the identity cosine distance and identity perceptual loss as defined in [43]. Finally, we obtain accurate illumination and facial expression parameters by penalizing the disparity between the per-pixel color intensity and the 3D facial landmarks using $\mathcal{G}_{mse} = \|\mathbf{I}_0 - \mathbf{I}\|_2$ and $\mathcal{G}_{lan} = \|\mathcal{M}(\mathbf{I}_0) - \mathcal{M}(\mathbf{I})\|_2$ respectively.

4. Experiments

4.1. Dataset

Training such a diffusion model in a supervised manner requires a large dataset of labeled sets of facial images \mathbf{I} , facial textures \mathbf{T} , shape parameters \mathbf{z}_{shp} and facial recognition embeddings \mathbf{V} . Although a captured dataset could be used, there are no large enough public datasets [103]. As a workaround, we manually picked 9K 2D facial images from the CelebA-HQ Dataset [35] $\mathbf{I}_i, i = 0 \dots 9 \cdot 10^3$, on which we performed the following steps to acquire the

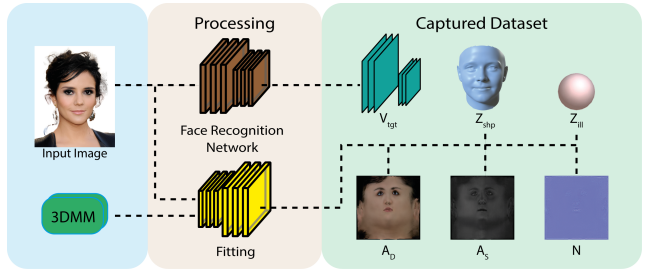


Figure 5. Dataset Acquisition: After fitting a trained facial reconstruction network [43] on images from CeleA-HQ Dataset [35], we create a synthetic dataset consisting of identity embedding vectors \mathbf{V}_{tgt} , diffuse \mathbf{A}_D and specular \mathbf{A}_S albedos, normals \mathbf{N} , PCA blends \mathbf{z}_{shp} and scene illumination \mathbf{z}_{ill} .

labeled dataset: A) We use a state-of-the-art face recognition model [16], to extract the identity latent embeddings \mathbf{V} , which captures the facial structure, with minimal interference from shading, age, and accessories. B) We train a state-of-the-art StyleGAN-based [38] facial reconstruction network [43] ϕ , on public datasets of facial textures [41, 59], and use the LSFM 3DMM for the facial shape [9]. Following an iterative optimization [43], we fit our model to the CelebA-HQ dataset [35] and acquire pseudo-ground truth facial textures, 3DMM shape weights, and scene illumination parameters $\phi(\mathbf{I}_i) \rightarrow \mathbf{A}_{D_i}, \mathbf{A}_{S_i}, \mathbf{N}_i, \mathbf{z}_{shp_i}, \mathbf{z}_{ill_i}$. In the end, we acquire a dataset of paired images, facial reflectance textures, facial shape, scene illumination and latent vectors: $\{\mathbf{I}_i, \mathbf{A}_{D_i}, \mathbf{A}_{S_i}, \mathbf{N}_i, \mathbf{z}_{shp_i}, \mathbf{z}_{ill_i}, \mathbf{V}_i\}$.

4.2. Unconditional Sampling

As mentioned in Sec. 3.3, FitDiff is trained following the classifier-free guidance (CFG) [31] training scheme. In this manner, our method can generate completely random facial identities without any prior input or supervision. We present the unconditional generated diffuse albedos \mathbf{A}_D , specular albedos \mathbf{A}_S , normals \mathbf{N} , facial shapes \mathbf{S} and renderings in Fig. 6. This figure illustrates our method’s ability to cre-

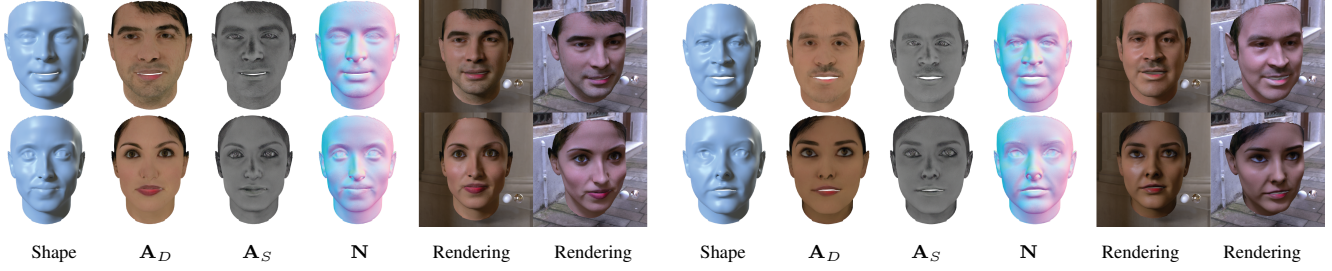


Figure 6. Samples generated by FitDiff with unconditional sampling. Our method can generate diverse facial shapes and reflectance maps.

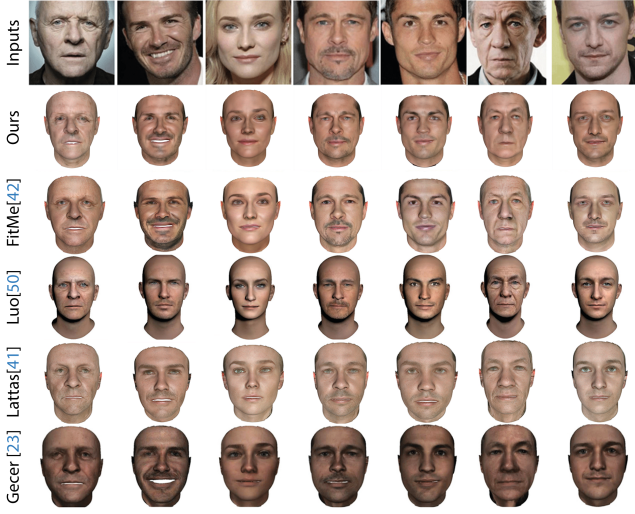


Figure 7. Qualitative comparison between our method and other monocular-image facial reconstruction approaches [24, 42, 43, 51]

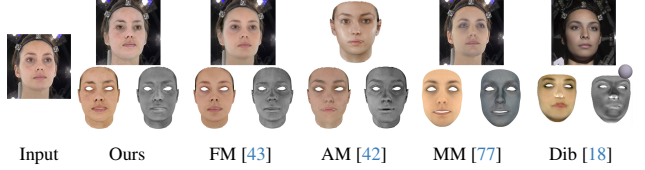
ate distinct shapes and textures. These assets hold significant potential for various applications, including enhancing existing datasets through augmentation and enrichment, as well as generating truly random identities for computer-based applications.

4.3. Qualitative comparisons

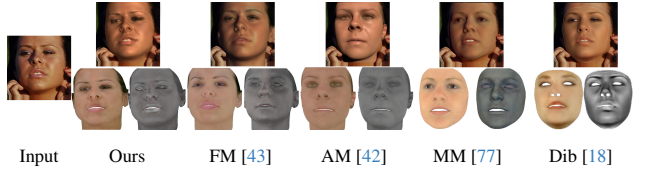
We compare our method’s generated samples with other monocular-image face reconstruction methods [24, 42, 43, 51] and present the generated samples in Fig. 7. The majority of these techniques rely on GAN-based methods and employ fitting optimization procedures that encompass lighting, camera pose, and expression parameters. Our method can capture finer details than most of GAN-based methods [24, 42, 43, 51]).

4.4. Quantitative comparisons

One of the key elements of our model is the ability to generate the facial identity depicted in the provided “in-the-wild” image. We quantitatively measure this by conducting an identity preservation experiment [22, 24, 27, 28]. We reconstruct the facial identities depicted in each image



(a) Comparison on Digital Emily [1].



(b) Comparison on a challenging case from Dib et al. [18].

Figure 8. Qualitative comparison on single-image reflectance acquisition against FitMe (FM) [42], AvatarMe++ (AM) [42], AlbedoMM (MM) [77] and Dib et al. [18]. Left: overlaid rendering, Up: diffuse, Down: specular.

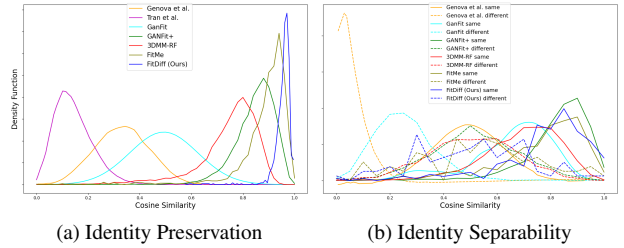


Figure 9. Identity preservation experiments: We compare our approach with other face-reconstruction networks [22, 24, 27, 28, 43, 87] and we achieve state-of-the-art identity preservation results.

within the Labeled Faces in the Wild (LFW) dataset [34]. The reconstructed identities are fed into a face recognition network [62] and the identity cosine distance is measured by comparing their activation layers. On top of that, our method’s ability to preserve the identity embeddings between the same people is measured by comparing predefined pairs containing the same and different people. As depicted in Fig. 9, FitDiff outperforms the previous state-of-the-art face-reconstruction methods [24, 43]. Regardless of the scene conditions, FitDiff exhibits superior performance by accurately reconstructing the same identities and effec-

	Diffuse Albedo			Specular Albedo			Normals		
	↓MSE	↑PSNR	↑SSIM	↓MSE	↑PSNR	↑SSIM	↓MSE	↑PSNR	↑SSIM
MM [77]	0.028	15.82	0.595	0.007	21.24	0.608	-	-	-
AM [42]	0.014	18.30	0.635	0.005	19.77	0.640	0.002	27.26	0.723
FM [43]	0.009	21.12	0.645	0.004	23.95	0.642	0.002	26.77	0.719
Ours	0.009	21.16	0.647	0.004	24.30	0.645	0.001	28.74	0.734

Table 1. Quantitative comparison on 6 Light-Stage-captured data [29], between our method, AlbedoMM [77] (MM), AvatarMe++[42] (AM) and FitMe[43] (FM), measuring MSE, PSNR, and SSIM. Our method surpasses prior work in most cases.

Method	Label Only	CFG (w=2)	CFG (w=9)	Guidance
ID Sim.	0.43	0.49	0.45	0.88

Table 2. Quantitative ablation study on the identity similarity [16] performance of our method, with and without identity guidance.

tively distinguishing between different identities.

4.5. Facial Reflectance Acquisition Comparison

We evaluate the quality of our method’s generated facial reflectance maps by reconstructing 6 test subjects captured with a Light Stage [29]. We compare the generated diffuse albedos \mathbf{A}_D , specular albedos \mathbf{A}_S and normals \mathbf{N} with the respective ground truth, and MSE, PSNR, and SSIM distances are measured. We compare our method’s performance with AlbedoMM [77], AvatarMe++ [42] and FitMe [43] and the results are presented in Tab. 1 and Fig. 8. FitDiff achieves superior performance for all three different facial reflectance maps.

5. Ablation Study

We perform ablation studies on the contribution of the guidance algorithm and identity conditioning.

5.1. Sampling guidance

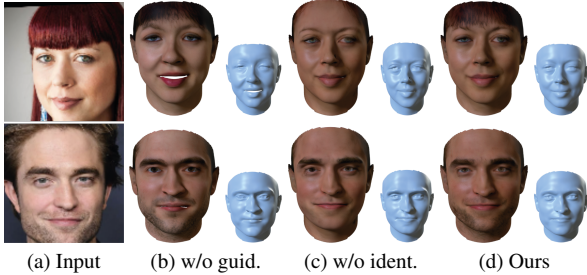


Figure 10. Ablation study: Given the input images in column a), we present corresponding samples without the guidance algorithm (b), without the identity embedding (c), and finally our method (d).

Firstly, we examine the importance of the proposed facial guidance during the reverse diffusion process. To do

so, we randomly pick about 100 “in-the-wild” images, and we consider three scenarios: a) sampling without any guidance, b) sampling using the classifier-free guidance [31] while using guidance scales $w = \{2, 9\}$, and C) our proposed method. The identity similarity scores are presented in Tab. 2, whereas visualizations of the generated examples are included in Fig. 10b. The guidance algorithm demonstrates superior reconstruction performance compared to alternative methodologies.

5.2. Use of the conditioning mechanism

Another ablation study includes the necessity of our conditioning mechanism. We compare the texture information between the generated samples with and without our conditioning mechanism and examples of those are presented in Fig. 10c and 10d, respectively. These examples clearly show that finer details can be generated only when the corresponding identity embedding is used as input.

6. Limitations and Future Work

In this work, we present the first-of-its-kind diffusion model that is conditioned on expressive facial embeddings, creating essentially a step towards a facial foundation model. Such models require vast datasets of labeled data [71], in our case paired facial images with geometry, reflectance and identity embeddings. These are immensely challenging to acquire in numbers, and hence we have to rely on a synthetic dataset and inherit its method’s limitations [43]. Nevertheless, our method could be trivially extended to larger datasets of even scanned datasets (e.g. [96]), given their availability. Moreover, the “fitting” nature of our method, is limited by the ambiguity between scene illumination and skin tone, especially in single-image inference. To that end, the recent method of TRUST [20], could be incorporated into our diffusion model, as an additional conditioning mechanism, given however the availability of training data.

7. Conclusion

In this paper, we introduced FitDiff, a diffusion-based 3D facial generative model, conditioned on identity embeddings. Acquiring such embeddings from a powerful pre-trained facial recognition method enables us to capture large variations in ethnicity, age, and gender from a single 2D facial image with no restriction on quality, pose, or illumination. Our method jointly generates facial shapes, facial reflectance maps, and scene illumination parameters. Through various experiments, FitDiff demonstrates its superior performance in preserving identity and reconstructing facial reflectance, surpassing existing methods. Finally, it exhibits the capability to generate unconditional samples, further highlighting its versatility and effectiveness.

Acknowledgements: S. Zafeiriou and part of the research was funded by the EPSRC Fellowship DEFORM (EP/S010203/1) and EPSRC Project GNOMON (EP/X011364/1).

References

- [1] Oleg Alexander, Mike Rogers, William Lambeth, Jen-Yuan Chiang, Wan-Chun Ma, Chuan-Chang Wang, and Paul Debevec. The digital emily project: Achieving a photorealistic digital actor. *IEEE Computer Graphics and Applications*, 30(4):20–31, 2010. [7](#)
- [2] Brian Amberg, Reinhard Knothe, and Thomas Vetter. Expression invariant 3D face recognition with a morphable model. In *2008 8th IEEE International Conference on Automatic Face and Gesture Recognition, FG 2008*, pages 1–6. IEEE, 2008. [3](#)
- [3] ShahRukh Athar, Zexiang Xu, Kalyan Sunkavalli, Eli Shechtman, and Zhixian Shu. Rignerv: Fully controllable neural 3d portraits. In *Computer Vision and Pattern Recognition (CVPR)*, 2022. [1](#), [3](#)
- [4] Timur Bagautdinov, Chenglei Wu, Jason Saragih, Pascal Fua, and Yaser Sheikh. Modeling facial geometry using compositional vaes. In *Proceedings of the IEEE Conference on Computer Vision and Pattern Recognition*, pages 3877–3886, 2018. [3](#)
- [5] Andrew D. Bagdanov, Alberto Del Bimbo, and Iacopo Masi. The florence 2d/3d hybrid face dataset. In *Proceedings of the 2011 Joint ACM Workshop on Human Gesture and Behavior Understanding*, page 79–80, New York, NY, USA, 2011. ACM. [2](#), [3](#)
- [6] Volker Blanz and Thomas Vetter. A morphable model for the synthesis of 3d faces. In *SIGGRAPH '99*, 1999. [1](#), [3](#)
- [7] Andreas Blattmann, Robin Rombach, Huan Ling, Tim Dockhorn, Seung Wook Kim, Sanja Fidler, and Karsten Kreis. Align your latents: High-resolution video synthesis with latent diffusion models. In *IEEE Conference on Computer Vision and Pattern Recognition (CVPR)*, 2023. [2](#), [3](#)
- [8] James Booth, Anastasios Roussos, Stefanos Zafeiriou, Allan Ponniah, and David Dunaway. A 3D morphable model learnt from 10,000 faces. In *Proceedings of the IEEE Computer Society Conference on Computer Vision and Pattern Recognition*, pages 5543–5552, 2016. [3](#), [2](#)
- [9] James Booth, Anastasios Roussos, Allan Ponniah, David Dunaway, and Stefanos Zafeiriou. Large scale 3d morphable models. *International Journal of Computer Vision*, 126(2):233–254, 2018. [2](#), [4](#), [5](#), [6](#)
- [10] Sofien Bouaziz, Yangang Wang, and Mark Pauly. Online modeling for realtime facial animation. *ACM Transactions on Graphics*, 32(4):40, 2013. [3](#)
- [11] Martin Breidt, Heinrich H. Biilthoff, and Cristobal Curio. Robust semantic analysis by synthesis of 3D facial motion. In *2011 IEEE International Conference on Automatic Face and Gesture Recognition and Workshops, FG 2011*, pages 713–719. IEEE, 2011. [3](#)
- [12] Adrian Bulat and Georgios Tzimiropoulos. How far are we from solving the 2d & 3d face alignment problem? (and a dataset of 230,000 3d facial landmarks). In *International Conference on Computer Vision*, 2017. [5](#), [6](#)
- [13] Chen Cao, Yanlin Weng, Shun Zhou, Yiyang Tong, and Kun Zhou. FaceWarehouse: A 3D facial expression database for visual computing. *IEEE Transactions on Visualization and Computer Graphics*, 20(3):413–425, 2014. [3](#)
- [14] Eric R. Chan, Connor Z. Lin, Matthew A. Chan, Koki Nagano, Boxiao Pan, Shalini De Mello, Orazio Gallo, Leonidas J. Guibas, Jonathan Tremblay, Sameh Khamis, Tero Karras, and Gordon Wetzstein. Efficient geometry-aware 3d generative adversarial networks. In *Proceedings of the IEEE/CVF Conference on Computer Vision and Pattern Recognition (CVPR)*, pages 16123–16133, 2022. [2](#), [3](#)
- [15] Hang Dai, Nick Pears, William Smith, and Christian Duncan. A 3D morphable model of craniofacial shape and texture variation. In *Proceedings of the IEEE International Conference on Computer Vision*, pages 3104–3112, 2017. [3](#)
- [16] Jiankang Deng, Jia Guo, Niannan Xue, and Stefanos Zafeiriou. Arcface: Additive angular margin loss for deep face recognition. In *Proceedings of the IEEE/CVF conference on computer vision and pattern recognition*, pages 4690–4699, 2019. [4](#), [5](#), [6](#), [8](#), [1](#)
- [17] Prafulla Dhariwal and Alexander Nichol. Diffusion models beat gans on image synthesis. In *Advances in Neural Information Processing Systems*, pages 8780–8794. Curran Associates, Inc., 2021. [2](#), [3](#), [4](#), [5](#)
- [18] Abdallah Dib, Cedric Thebault, Junghyun Ahn, Philippe-Henri Gosselin, Christian Theobalt, and Louis Chevallier. Towards high fidelity monocular face reconstruction with rich reflectance using self-supervised learning and ray tracing. In *Proceedings of the IEEE/CVF International Conference on Computer Vision*, pages 12819–12829, 2021. [3](#), [7](#)
- [19] Patrick Esser, Robin Rombach, and Bjorn Ommer. Taming transformers for high-resolution image synthesis. In *Proceedings of the IEEE/CVF Conference on Computer Vision and Pattern Recognition (CVPR)*, pages 12873–12883, 2021. [2](#), [4](#), [1](#)
- [20] Haiwen Feng, Timo Bolkart, Joachim Tesch, Michael J. Black, and Victoria Abrevaya. Towards racially unbiased skin tone estimation via scene disambiguation. In *European Conference on Computer Vision*, 2022. [8](#)
- [21] Yao Feng, Haiwen Feng, Michael J. Black, and Timo Bolkart. Learning an animatable detailed 3d face model from in-the-wild images. *ACM Trans. Graph.*, 40(4), 2021. [3](#)
- [22] Stathis Galanakis, Baris Gecer, Alexandros Lattas, and Stefanos Zafeiriou. 3dmm-rf: Convolutional radiance fields for 3d face modeling. In *Proceedings of the IEEE/CVF Winter Conference on Applications of Computer Vision (WACV)*, pages 3536–3547, 2023. [2](#), [3](#), [4](#), [7](#)
- [23] Chen Gao, Yichang Shih, Wei-Sheng Lai, Chia-Kai Liang, and Jia-Bin Huang. Portrait neural radiance fields from a single image. *arXiv preprint arXiv:2012.05903*, 2020. [2](#), [3](#)

- [24] Baris Gecer, Stylianos Ploumpis, Irene Kotsia, and Stefanos Zafeiriou. Ganfit: Generative adversarial network fitting for high fidelity 3d face reconstruction. In *Proceedings of the IEEE/CVF Conference on Computer Vision and Pattern Recognition (CVPR)*, 2019. 1, 2, 3, 5, 7
- [25] Baris Gecer, Alexander Lattas, Stylianos Ploumpis, Jiankang Deng, Athanasios Papaioannou, Stylianos Moschoglou, and Stefanos Zafeiriou. Synthesizing Coupled 3D Face Modalities by Trunk-Branch Generative Adversarial Networks. In *European Conference on Computer Vision (ECCV)*, 2020. 3
- [26] Baris Gecer, Jiankang Deng, and Stefanos Zafeiriou. Osetec: One-shot texture completion. In *Proceedings of the IEEE/CVF Conference on Computer Vision and Pattern Recognition (CVPR)*, pages 7628–7638, 2021. 2
- [27] Baris Gecer, Stylianos Ploumpis, Irene Kotsia, and Stefanos P Zafeiriou. Fast-ganfit: Generative adversarial network for high fidelity 3d face reconstruction. *IEEE Transactions on Pattern Analysis and Machine Intelligence*, 2021. 2, 3, 7, 1
- [28] Kyle Genova, Forrester Cole, Aaron Maschinot, Aaron Sarna, Daniel Vlasic, and William T. Freeman. Unsupervised training for 3d morphable model regression. In *Proceedings of the IEEE Conference on Computer Vision and Pattern Recognition (CVPR)*, 2018. 7, 1, 2, 3
- [29] Abhijeet Ghosh, Graham Fyffe, Borom Tunwattanapong, Jay Busch, Xueming Yu, and Paul Debevec. Multiview face capture using polarized spherical gradient illumination. *ACM Transactions on Graphics (TOG)*, 30(6):1–10, 2011. 8
- [30] Ian Goodfellow, Jean Pouget-Abadie, Mehdi Mirza, Bing Xu, David Warde-Farley, Sherjil Ozair, Aaron Courville, and Yoshua Bengio. Generative adversarial nets. In *Advances in Neural Information Processing Systems*. Curran Associates, Inc., 2014. 2
- [31] Jonathan Ho and Tim Salimans. Classifier-free diffusion guidance. *arXiv preprint arXiv:2207.12598*, 2022. 3, 5, 6, 8
- [32] Jonathan Ho, Ajay Jain, and Pieter Abbeel. Denoising diffusion probabilistic models. *arXiv preprint arxiv:2006.11239*, 2020. 2, 4
- [33] Yang Hong, Bo Peng, Haiyao Xiao, Ligang Liu, and Juyong Zhang. Headnerf: A real-time nerf-based parametric head model. 2022. 2, 3
- [34] Gary B. Huang, Manu Ramesh, Tamara Berg, and Erik Learned-Miller. Labeled faces in the wild: A database for studying face recognition in unconstrained environments. Technical Report 07-49, University of Massachusetts, Amherst, 2007. 7
- [35] Tero Karras, Timo Aila, Samuli Laine, and Jaakko Lehtinen. Progressive growing of GANs for improved quality, stability, and variation. In *International Conference on Learning Representations*, 2018. 2, 6
- [36] Tero Karras, Samuli Laine, and Timo Aila. A style-based generator architecture for generative adversarial networks. *CoRR*, abs/1812.04948, 2018. 2
- [37] Tero Karras, Miika Aittala, Janne Hellsten, Samuli Laine, Jaakko Lehtinen, and Timo Aila. Training generative adversarial networks with limited data. In *Proc. NeurIPS*, 2020.
- [38] Tero Karras, Samuli Laine, Miika Aittala, Janne Hellsten, Jaakko Lehtinen, and Timo Aila. Analyzing and improving the image quality of StyleGAN. In *Proc. CVPR*, 2020. 2, 6
- [39] Gwanghyun Kim, Taesung Kwon, and Jong Chul Ye. Diffusionclip: Text-guided diffusion models for robust image manipulation. In *Proceedings of the IEEE/CVF Conference on Computer Vision and Pattern Recognition (CVPR)*, pages 2426–2435, 2022. 3
- [40] Naveen Kodali, Jacob Abernethy, James Hays, and Zsolt Kira. On convergence and stability of gans. *arXiv preprint arXiv:1705.07215*, 2017. 2
- [41] Alexandros Lattas, Stylianos Moschoglou, Baris Gecer, Stylianos Ploumpis, Vasileios Triantafyllou, Abhijeet Ghosh, and Stefanos Zafeiriou. Avatarme: Realistically renderable 3d facial reconstruction ”in-the-wild”. In *Proceedings of the IEEE/CVF Conference on Computer Vision and Pattern Recognition (CVPR)*, 2020. 1, 2, 3, 6
- [42] Alexandros Lattas, Stylianos Moschoglou, Stylianos Ploumpis, Baris Gecer, Abhijeet Ghosh, and Stefanos P Zafeiriou. Avatarme++: Facial shape and brdf inference with photorealistic rendering-aware gans. *IEEE Transactions on Pattern Analysis & Machine Intelligence*, (01):1–1, 2021. 2, 3, 5, 6, 7, 8
- [43] Alexandros Lattas, Stylianos Moschoglou, Stylianos Ploumpis, Baris Gecer, Jiankang Deng, and Stefanos Zafeiriou. FitMe: Deep photorealistic 3D morphable model avatars. In *Proceedings of the IEEE/CVF Conference on Computer Vision and Pattern Recognition (CVPR)*, 2023. 2, 3, 4, 5, 6, 7, 8, 1
- [44] Chunlu Li, Andreas Morel-Forster, Thomas Vetter, Bernhard Egger, and Adam Kortylewski. Robust model-based face reconstruction through weakly-supervised outlier segmentation. In *Proceedings of the IEEE/CVF Conference on Computer Vision and Pattern Recognition*, pages 372–381, 2023. 2
- [45] Hao Li, Thibaut Weise, and Mark Pauly. Example-based facial rigging. *ACM SIGGRAPH 2010 Papers, SIGGRAPH 2010*, 29(4):32, 2010. 3
- [46] Tianye Li, Timo Bolkart, Michael J. Black, Hao Li, and Javier Romero. Learning a model of facial shape and expression from 4D scans. *ACM Transactions on Graphics, (Proc. SIGGRAPH Asia)*, 36(6):194:1–194:17, 2017. 2, 3
- [47] Chen-Hsuan Lin, Jun Gao, Luming Tang, Towaki Takikawa, Xiaohui Zeng, Xun Huang, Karsten Kreis, Sanja Fidler, Ming-Yu Liu, and Tsung-Yi Lin. Magic3d: High-resolution text-to-3d content creation. In *Proceedings of the IEEE/CVF Conference on Computer Vision and Pattern Recognition (CVPR)*, pages 300–309, 2023. 3
- [48] Haohe Liu, Zehua Chen, Yi Yuan, Xinhao Mei, Xubo Liu, Danilo Mandic, Wenwu Wang, and Mark D Plumbley. Audioldm: Text-to-audio generation with latent diffusion models. *arXiv preprint arXiv:2301.12503*, 2023. 2, 3
- [49] Zhen Liu, Yao Feng, Michael J. Black, Derek Nowrouzezahrai, Liam Paull, and Weiyang Liu. Meshdiffusion: Score-based generative 3d mesh modeling. In

- International Conference on Learning Representations*, 2023. 3
- [50] Stephen Lombardi, Jason Saragih, Tomas Simon, and Yaser Sheikh. Deep appearance models for face rendering. *ACM Transactions on Graphics*, 37(4):68, 2018. 3
- [51] Huiwen Luo, Koki Nagano, Han-Wei Kung, Qingguo Xu, Zejian Wang, Lingyu Wei, Liwen Hu, and Hao Li. Normalized avatar synthesis using stylegan and perceptual refinement. In *Proceedings of the IEEE/CVF Conference on Computer Vision and Pattern Recognition (CVPR)*, pages 11662–11672, 2021. 3, 7
- [52] Zhaoyang Lyu, Zhifeng Kong, Xudong Xu, Liang Pan, and Dahua Lin. A conditional point diffusion-refinement paradigm for 3d point cloud completion. *ArXiv*, abs/2112.03530, 2021. 3
- [53] Zhiyuan Ma, Xiangyu Zhu, Guojun Qi, Zhen Lei, and Lei Zhang. Otavatar: One-shot talking face avatar with controllable tri-plane rendering. *arXiv preprint arXiv:2303.14662*, 2023. 1, 3
- [54] Ben Mildenhall, Pratul P Srinivasan, Matthew Tancik, Jonathan T Barron, Ravi Ramamoorthi, and Ren Ng. Nerf: Representing scenes as neural radiance fields for view synthesis. In *European conference on computer vision*, pages 405–421. Springer, 2020. 3
- [55] Shakir Mohamed and Balaji Lakshminarayanan. Learning in implicit generative models. *arXiv preprint arXiv:1610.03483*, 2016. 5
- [56] Stylianos Moschoglou, Stylianos Ploumpis, Mihalys Nicolaou, Athanasios Papaioannou, and Stefanos Zafeiriou. 3DFaceGAN: Adversarial nets for 3D face representation, generation, and translation. *arXiv preprint arXiv:1905.00307*, 2019. 3
- [57] Alex Nichol, Pratul P Dhariwal, Aditya Ramesh, Pranav Shyam, Pamela Mishkin, Bob McGrew, Ilya Sutskever, and Mark Chen. Glide: Towards photorealistic image generation and editing with text-guided diffusion models. *arXiv preprint arXiv:2112.10741*, 2021. 3
- [58] Roy Or-El, Xuan Luo, Mengyi Shan, Eli Shechtman, Jeong Joon Park, and Ira Kemelmacher-Shlizerman. Stylesdf: High-resolution 3d-consistent image and geometry generation. In *Proceedings of the IEEE/CVF Conference on Computer Vision and Pattern Recognition (CVPR)*, pages 13503–13513, 2022. 2, 3
- [59] Athanasios Papaioannou, Baris Gecer, Shiyang Cheng, Grigorios Chrysos, Jiankang Deng, Eftychia Fotiadou, Christos Kampouris, Dimitrios Kollias, Stylianos Moschoglou, Kritaphat Songsri-In, et al. Mimicme: A large scale diverse 4d database for facial expression analysis. In *Computer Vision—ECCV 2022: 17th European Conference, Tel Aviv, Israel, October 23–27, 2022, Proceedings, Part VIII*, pages 467–484. Springer, 2022. 6
- [60] Jeong Joon Park, Peter Florence, Julian Straub, Richard Newcombe, and Steven Lovegrove. DeepSDF: Learning continuous signed distance functions for shape representation. In *The IEEE Conference on Computer Vision and Pattern Recognition (CVPR)*, 2019. 3
- [61] Taesung Park, Ming-Yu Liu, Ting-Chun Wang, and Jun-Yan Zhu. Semantic image synthesis with spatially-adaptive normalization. In *Proceedings of the IEEE Conference on Computer Vision and Pattern Recognition*, 2019. 3, 4, 1
- [62] Omkar M. Parkhi, Andrea Vedaldi, and Andrew Zisserman. Deep face recognition. In *Proceedings of the British Machine Vision Conference (BMVC)*, pages 41.1–41.12. BMVA Press, 2015. 7
- [63] Pascal Paysan, Reinhard Knothe, Brian Amberg, Sami Romdhani, and Thomas Vetter. A 3D Face Model for Pose and Illumination Invariant Face Recognition. In *2009 Sixth IEEE International Conference on Advanced Video and Signal Based Surveillance*, pages 296–301, 2009. 2, 3
- [64] Walter H. L. Pinaya, Petru-Daniel Tudosiu, Jessica Dafflon, Pedro F. Da Costa, Virginia Fernandez, Parashkev Nachev, Sebastien Ourselin, and M. Jorge Cardoso. Brain imaging generation with latent diffusion models. In *Deep Generative Models*, pages 117–126, Cham, 2022. Springer Nature Switzerland. 2, 3
- [65] Ben Poole, Ajay Jain, Jonathan T. Barron, and Ben Mildenhall. Dreamfusion: Text-to-3d using 2d diffusion. *arXiv*, 2022. 3
- [66] Alec Radford, Jong Wook Kim, Chris Hallacy, A. Ramesh, Gabriel Goh, Sandhini Agarwal, Girish Sastry, Amanda Askell, Pamela Mishkin, Jack Clark, Gretchen Krueger, and Ilya Sutskever. Learning transferable visual models from natural language supervision. In *ICML*, 2021. 2
- [67] Aditya Ramesh, Mikhail Pavlov, Gabriel Goh, Scott Gray, Chelsea Voss, Alec Radford, Mark Chen, and Ilya Sutskever. Zero-shot text-to-image generation. *CoRR*, abs/2102.12092, 2021. 3
- [68] Anurag Ranjan, Timo Bolkart, Soubhik Sanyal, and Michael J. Black. Generating 3D faces using convolutional mesh autoencoders. *Lecture Notes in Computer Science (including subseries Lecture Notes in Artificial Intelligence and Lecture Notes in Bioinformatics)*, 11207 LNCS:725–741, 2018. 3
- [69] Nikhila Ravi, Jeremy Reizenstein, David Novotny, Taylor Gordon, Wan-Yen Lo, Justin Johnson, and Georgia Gkioxari. Accelerating 3d deep learning with pytorch3d. *arXiv:2007.08501*, 2020. 5
- [70] Daniel Roich, Ron Mokady, Amit H Bermano, and Daniel Cohen-Or. Pivotal tuning for latent-based editing of real images. *ACM Trans. Graph.*, 2021. 2
- [71] Robin Rombach, Andreas Blattmann, Dominik Lorenz, Patrick Esser, and Björn Ommer. High-resolution image synthesis with latent diffusion models. In *Proceedings of the IEEE/CVF Conference on Computer Vision and Pattern Recognition (CVPR)*, pages 10684–10695, 2022. 2, 3, 4, 5, 8, 1
- [72] Olaf Ronneberger, Philipp Fischer, and Thomas Brox. U-net: Convolutional networks for biomedical image segmentation. *CoRR*, abs/1505.04597, 2015. 4
- [73] Tim Salimans, Ian Goodfellow, Wojciech Zaremba, Vicki Cheung, Alec Radford, Xi Chen, and Xi Chen. Improved techniques for training gans. In *Advances in Neural Information Processing Systems*. Curran Associates, Inc., 2016. 2

- [74] Florian Schroff, Dmitry Kalenichenko, and James Philbin. Facenet: A unified embedding for face recognition and clustering. In *Proceedings of the IEEE Conference on Computer Vision and Pattern Recognition (CVPR)*, 2015. 6
- [75] Sahil Sharma and Vijay Chahar. 3d face reconstruction in deep learning era: A survey. *Archives of Computational Methods in Engineering*, 2022. 3
- [76] Abhishek Sinha, Jiaming Song, Chenlin Meng, and Stefano Ermon. D2c: Diffusion-decoding models for few-shot conditional generation. *Advances in Neural Information Processing Systems*, 34:12533–12548, 2021. 3
- [77] William A. P. Smith, Alassane Seck, Hannah Dee, Bernard Tiddeman, Joshua Tenenbaum, and Bernhard Egger. A Morphable Face Albedo Model. *arXiv:2004.02711 [cs]*, 2020. 3, 7, 8
- [78] Jascha Sohl-Dickstein, Eric A. Weiss, Niru Maheswaranathan, and Surya Ganguli. Deep unsupervised learning using nonequilibrium thermodynamics. *32nd International Conference on Machine Learning, ICML 2015*, 3:2246–2255, 2015. 2, 3
- [79] Jiaming Song, Chenlin Meng, and Stefano Ermon. Denoising diffusion implicit models. *arXiv:2010.02502*, 2020. 3, 5
- [80] Yang Song and Stefano Ermon. Generative modeling by estimating gradients of the data distribution. *Advances in neural information processing systems*, 32, 2019. 3
- [81] Yang Song and Stefano Ermon. Improved techniques for training score-based generative models. *Advances in neural information processing systems*, 33:12438–12448, 2020.
- [82] Yang Song, Jascha Sohl-Dickstein, Diederik P Kingma, Abhishek Kumar, Stefano Ermon, and Ben Poole. Score-based generative modeling through stochastic differential equations. In *International Conference on Learning Representations*, 2021. 3, 5
- [83] Giota Stratou, Abhijeet Ghosh, Paul Debevec, and Louis-Philippe Morency. Effect of illumination on automatic expression recognition: a novel 3D relightable facial database. In *Proc. International Conference on Automatic Face and Gesture Recognition*, pages 611–618, 2011. 2
- [84] Ayush Tewari, Florian Bernard, Pablo Garrido, Gaurav Bharaj, Mohamed Elgharib, Hans-Peter Seidel, Patrick Perez, Michael Zollhofer, and Christian Theobalt. FML: Face Model Learning From Videos. In *2019 IEEE/CVF Conference on Computer Vision and Pattern Recognition (CVPR)*, pages 10804–10814, Long Beach, CA, USA, 2019. IEEE. 3
- [85] Hoang Thanh-Tung and Truyen Tran. Catastrophic forgetting and mode collapse in gans. In *2020 international joint conference on neural networks (ijcnn)*, pages 1–10. IEEE, 2020. 3
- [86] Justus Thies, Michael Zollhöfer, Matthias Nießner, Levi Valgaerts, Marc Stamminger, and Christian Theobalt. Real-time expression transfer for facial reenactment. *ACM Transactions on Graphics*, 34(6):181–183, 2015. 3
- [87] Anh Tuan Tran, Tal Hassner, Iacopo Masi, and Gérard Medioni. Regressing robust and discriminative 3D morphable models with a very deep neural network. In *Proceedings - 30th IEEE Conference on Computer Vision and Pattern Recognition, CVPR 2017*, pages 1493–1502, 2017. 7, 2, 3
- [88] Luan Tran and Xiaoming Liu. On learning 3D face morphable model from in-the-wild images. *IEEE Transactions on Pattern Analysis and Machine Intelligence*, pages 1–1, 2019. 3
- [89] Arash Vahdat, Karsten Kreis, and Jan Kautz. Score-based generative modeling in latent space. In *Neural Information Processing Systems (NeurIPS)*, 2021. 2, 3
- [90] Ashish Vaswani, Noam Shazeer, Niki Parmar, Jakob Uszkoreit, Llion Jones, Aidan N Gomez, Łukasz Kaiser, and Illia Polosukhin. Attention is all you need. In *Advances in Neural Information Processing Systems*. Curran Associates, Inc., 2017. 4
- [91] Tengfei Wang, Bo Zhang, Ting Zhang, Shuyang Gu, Jianmin Bao, Tadas Baltrušaitis, Jingjing Shen, Dong Chen, Fang Wen, Qifeng Chen, et al. Rodin: A generative model for sculpting 3d digital avatars using diffusion. *arXiv preprint arXiv:2212.06135*, 2022. 2, 3
- [92] Shih En Wei, Jason Saragih, Tomas Simon, Adam W. Harley, Stephen Lombardi, Michal Perdoch, Alexander Hypes, Dawei Wang, Hernan Badino, and Yaser Sheikh. VR facial animation via multiview image translation. *ACM Transactions on Graphics*, 38(4):67, 2019. 3
- [93] Erroll Wood, Tadas Baltrušaitis, Charlie Hewitt, Matthew Johnson, Jingjing Shen, Nikola Milosavljević, Daniel Wilde, Stephan Garbin, Toby Sharp, Ivan Stojiljković, et al. 3d face reconstruction with dense landmarks. In *European Conference on Computer Vision*, pages 160–177. Springer, 2022. 3
- [94] Jay Zhangjie Wu, Yixiao Ge, Xintao Wang, Stan Weixian Lei, Yuchao Gu, Yufei Shi, Wynne Hsu, Ying Shan, Xiaohu Qie, and Mike Zheng Shou. Tune-a-video: One-shot tuning of image diffusion models for text-to-video generation. In *Proceedings of the IEEE/CVF International Conference on Computer Vision (ICCV)*, pages 7623–7633, 2023. 3
- [95] Fei Yang, Dimitri Metaxas, Jue Wang, Eli Shechtman, and Lubomir Bourdev. Expression flow for 3D-Aware face component transfer. *ACM Transactions on Graphics*, 30(4):1–10, 2011. 3
- [96] Haotian Yang, Hao Zhu, Yanru Wang, Mingkai Huang, Qiu Shen, Ruigang Yang, and Xun Cao. Facescape: a large-scale high quality 3d face dataset and detailed riggable 3d face prediction. In *Proceedings of the IEEE/CVF Conference on Computer Vision and Pattern Recognition*, pages 601–610, 2020. 8
- [97] Tarun Yenamandra, Ayush Tewari, Florian Bernard, Hans-Peter Seidel, Mohamed Elgharib, Daniel Cremers, and Christian Theobalt. i3dmm: Deep implicit 3d morphable model of human heads. In *Proceedings of the IEEE/CVF Conference on Computer Vision and Pattern Recognition*, pages 12803–12813, 2021. 3
- [98] Xiaohui Zeng, Arash Vahdat, Francis Williams, Zan Gojcic, Or Litany, Sanja Fidler, and Karsten Kreis. Lion: Latent point diffusion models for 3d shape generation. In *Advances in Neural Information Processing Systems (NeurIPS)*, 2022. 3

- [99] Longwen Zhang, Qiwei Qiu, Hongyang Lin, Qixuan Zhang, Cheng Shi, Wei Yang, Ye Shi, Sibe Yang, Lan Xu, and Jingyi Yu. Dreamface: Progressive generation of animatable 3d faces under text guidance. *arXiv preprint arXiv:2304.03117*, 2023. 2, 3
- [100] Richard Zhang, Phillip Isola, Alexei A Efros, Eli Shechtman, and Oliver Wang. The unreasonable effectiveness of deep features as a perceptual metric. In *CVPR*, 2018. 4
- [101] Linqi Zhou, Yilun Du, and Jiajun Wu. 3d shape generation and completion through point-voxel diffusion. In *Proceedings of the IEEE/CVF International Conference on Computer Vision (ICCV)*, pages 5826–5835, 2021. 3
- [102] Yiyu Zhuang, Hao Zhu, Xusen Sun, and Xun Cao. Mofan-erf: Morphable facial neural radiance field. *arXiv preprint arXiv:2112.02308*, 2021. 2
- [103] Wojciech Zielonka, Timo Bolkart, and Justus Thies. Towards metrical reconstruction of human faces. In *European Conference on Computer Vision*, pages 250–269. Springer, 2022. 1, 3, 6

FitDiff: Robust monocular 3D facial shape and reflectance estimation using Diffusion Models

Supplementary Material

A. Implementation Details

In this section, we provide the essential information required to reproduce our method comprehensively. The code-base for the brached multi-modal AutoEncoder is built on the public repository of the VQGAN AutoEncoder [19]. We made the following changes: A) The first downsampling layer of the encoder \mathcal{E} and the last upsampling layer of the decoder \mathcal{D} are branched, by making 3 copies of the respective layers. B) As proposed in FitMe [43], we use a branched discriminator, in the essence of having 2 copies of the main discriminator, except the last convolutional layer. The branch, dedicated for diffuse (\mathbf{A}_D) and specular (\mathbf{A}_S) albedos, gets a 6-channel input whereas the normals (\mathbf{N}) branch gets a 3-channel input.

f	$ \mathcal{Z} $	Embed. dim
8	16384	1
z channels	Channels	Channels mult.
4	128	1,2,2,4
Res. Blocks	Attention Res.	Batch Size
2	32	16

Table 3. Hype-parameters used during training the branched multi-modal AutoEncoder.

On the other hand, the main training phase is built on the public repository of Latent Diffusion Models [71]. We modified the provided UNet code by turning it into a 1-D UNet network and replaced the attention-based conditional mechanism with SPADE layers [61]. The hyper-parameters for the Condinional UNet using SPADE layers are presented in Tab. 4 while it gets trained for 800 epochs.

Diffusion steps	Noise Schedule	Input Channels
1000	linear	1
Channels	Cond. Dim	SPADE dim.
192	1048	128
Channels mult	Depth	Heads
1,2,4,8	2	4
Heads Channels	Batch size	LR
32	16	3.2e-05

Table 4. Hyper-parameters of the main training phase.

A.1. Definition of training losses

We penalize the differences between the ground truth and the estimated identity vectors and shapes, by using the fol-

lowing losses:

Identity Cosine Distance Following [27, 28, 43] the identity features are extracted by a face recognition network [16] and their distance is penalized by the formula:

$$L_{id} := \mathbb{E}_{\bar{\mathbf{I}}_0} \left[1 - \frac{\mathcal{F}^n(\bar{\mathbf{I}}_0) \cdot \mathcal{F}^n(\mathbf{I})}{\|\mathcal{F}^n(\bar{\mathbf{I}}_0)\|_2 \cdot \|\mathcal{F}^n(\mathbf{I})\|_2} \right] \quad (3)$$

Identity Perceptual Loss As introduced in [43], let \mathcal{C}^i be the i -th intermediate layer of the used face recognition network [16]. We also penalize the distance between the intermediate activation layers, in order to achieve perceptual consistency, by using the equation:

$$L_{per} := \mathbb{E}_{\bar{\mathbf{I}}_0} \left[\sum_j^n \frac{\|\mathcal{F}^j(\bar{\mathbf{I}}_0) - \mathcal{F}^j(\mathbf{I})\|_2}{H_{F^j} \cdot W_{F^j} \cdot C_{F^j}} \right] \quad (4)$$

Shape loss Finally, we achieve shape consistency between the ground truth and the estimated initial avatar, by the following distance formula:

$$L_{verts} := \mathbb{E}_{\bar{\mathbf{S}}_0} [\|\bar{\mathbf{S}}_0 - \mathbf{S}\|_1] \quad (5)$$

A.2. Guidance Algorithm

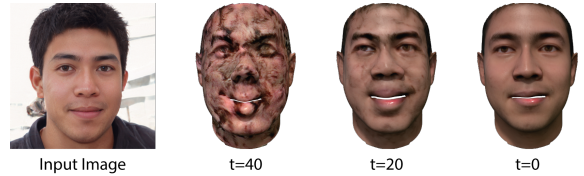


Figure 11. An example of the sampling process for $t = \{40, 20, 0\}$,

FitDiff is a diffusion-based architecture conditioned on an identity embedding vector. It accurately generates facial identities by incorporating an effective identity guidance method during the sampling phase. An example of this process is illustrated in Fig. 11. The proposed guidance method uses the guidance loss which is formulated as:

$$\mathcal{G} = \mathcal{G}_{id}^{cos} + \lambda_1 \mathcal{G}_{id}^{per} + \lambda_2 \mathcal{G}_{mse} + \lambda_3 \mathcal{G}_{lan} \quad (6)$$

The values of the used lambdas are $\lambda_1 = 50$, $\lambda_2 = 10$, $\lambda_3 = 200$ where we use a gradient scale $s = 90$. We run our sampling method for $T = 50$ steps. The diffusion sampling process takes about 54 secons when it runs on an NVIDIA Tesla V100-PCIE-32GB GPU.

B. Controlling the generated identity

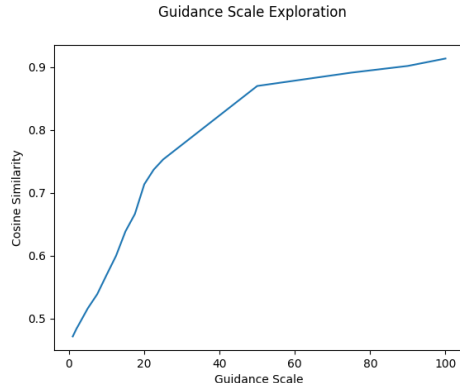


Figure 12. Guidance scale exploration: We randomly pick 10 facial images across the web. We measure the identity similarity between the ground truth image and the generated avatars for different guidance scales.

Choosing the guidance scale is an important factor for the trade-off between the intra-class diversity of the generated samples and the accuracy of the reconstruction. We conduct an experiment by choosing 10 “in-the-wild” images across the web and sample while using different guidance scales for a range of $s = [0, 100]$. We showcase the results in Fig. 12.

C. Partial Texture Completion

FitDiff finds another application in the domain of partial reflectance map completion, illustrated in Fig. 13. In certain scenarios, the input reflectance map may be provided partially completed. Due to the absence of ground truth facial reflectance maps and with the intention of demonstrating our model’s ability to complete partial texture maps, we examine the following scenario: Given the input images illustrated in Fig. 13a, we firstly reconstruct the corresponding facial identity (Fig. 13b and 13e). The resulting diffuse albedo images are treated as pseudo-ground truth and a part of it is randomly masked (Fig. 13c). Obtaining completed diffuse albedo maps involves sampling while using only the input identity embedding vector. The resulting diffuse albedos are showcased in Fig. 13d whilst the corresponding renderings are shown in Fig 13f. By comparing those figures, it is evident that FitDiff clearly retrieves the masked parts, effectively completing the partially visible reflectance maps.

D. Additional Results

D.1. Challenging Images

In this section, we demonstrate the robustness of our method in handling challenging images containing occlu-

sions, such as glasses and hairbands. In this manner, we reconstruct images from FitMe [43], and showcase the results in Fig. 14. The results, generated by FitMe, were provided by its authors and are presented in Fig. 14b. Notably, these images contain faded parts of the overlaid items (shown in a red box). This is due to the integrated pivotal tuning inversion (PTI) [70] employed during the fitting process. On the contrary, our method is not affected by those occlusions and generates clear texture maps (Fig. 14c).

D.2. MICC

We measure the ability of our network to accurately reconstruct the facial shape of individuals. Following the methods presented in [24, 43], we reconstruct the facial shape for each subject included in MICC Florence 3D Faces dataset (MICC) [5]. This dataset contains videos of 53 different individuals under 3 different category videos: “co-operative”, “indoor” and “outdoor”. We present our findings for each category separately, following the open-source benchmark code provided by the authors of GANFit [24]. We randomly pick 3 frames from each video and measure the point-to-plane distance between the ground truth and reconstructed facial shapes. The reconstruction results are shown in Tab. 5.

Our method performs about equal as the state-of-the-art networks in each different video category (GANFit [24], GANFit+ [27], FitMe [43]) while beating the rest (Tran [87], Booth [8], Genova [28]). Overall, GANFit+ [27] achieves slightly better performance than ours. This can be explained by the fact that our approach is trained by using synthetic data acquired from a fitting methodology [43]. This reliance on synthetic data imposes limitations on our method’s capability for shape retrieval, resulting in performance on par with FitMe [43]. Furthermore, as highlighted by the authors of FitMe, the concurrent reconstruction of both facial shape and texture normals introduces constraints on the approach’s shape reconstruction performance. Specifically, a portion of the shape information is occasionally encoded in the normals domain rather than in the actual facial shape domain.

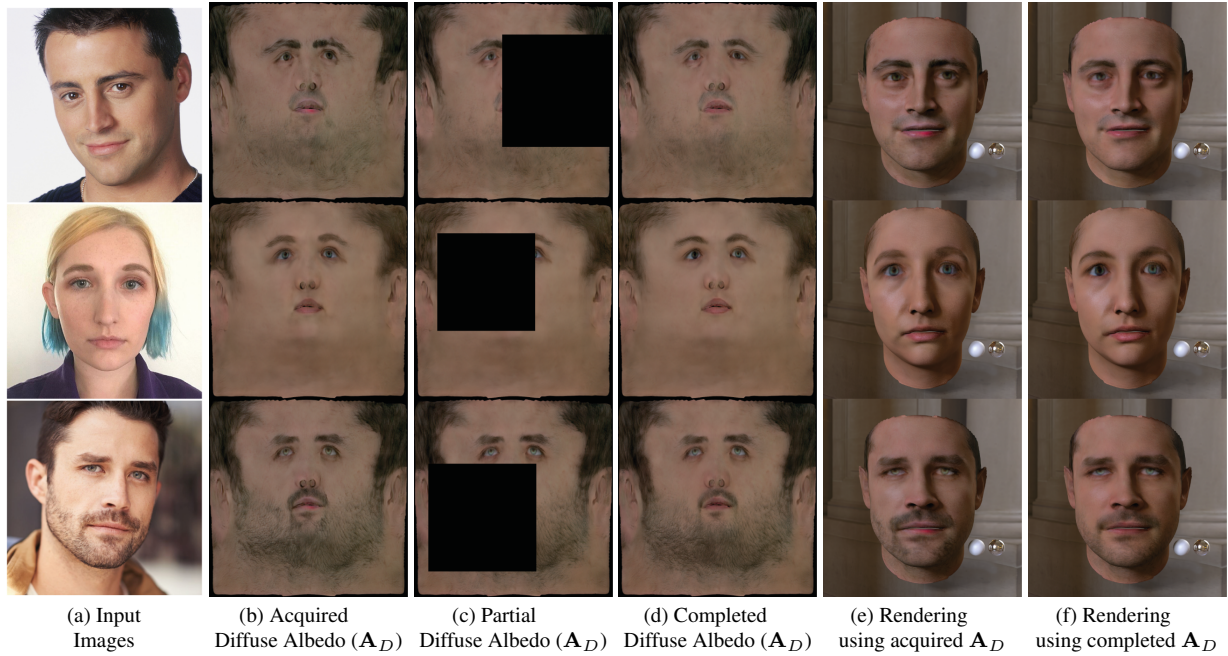


Figure 13. Our method can be used for facial texture completion.

Method	Cooperative Mean \pm Std.	Indoor Mean \pm Std.	Outdoor Mean \pm Std.
Tran et al.[87]	1.93 ± 0.27	2.02 ± 0.25	1.86 ± 0.24
Booth et al.[8]	1.82 ± 0.29	1.85 ± 0.22	1.63 ± 0.16
Genova et al.[28]	1.50 ± 0.14	1.50 ± 0.11	1.48 ± 0.11
GANFit[24]	0.95 ± 0.10	0.94 ± 0.10	0.94 ± 0.10
GANFit+ [27]	0.94 ± 0.17	0.92 ± 0.14	0.94 ± 0.19
FastGANFit [27]	1.11 ± 0.25	0.98 ± 0.15	1.16 ± 0.18
FitMe [43]	0.95 ± 0.18	0.97 ± 0.20	0.98 ± 0.21
FitDiff (Ours)	0.96 ± 0.17	0.98 ± 0.13	0.96 ± 0.15

Table 5. Quantitative comparison of shape reconstruction, on the MICC dataset [5] under three different video categories. We compare our method with [8, 24, 27, 28, 43, 87]. and we achieve comparable performance.

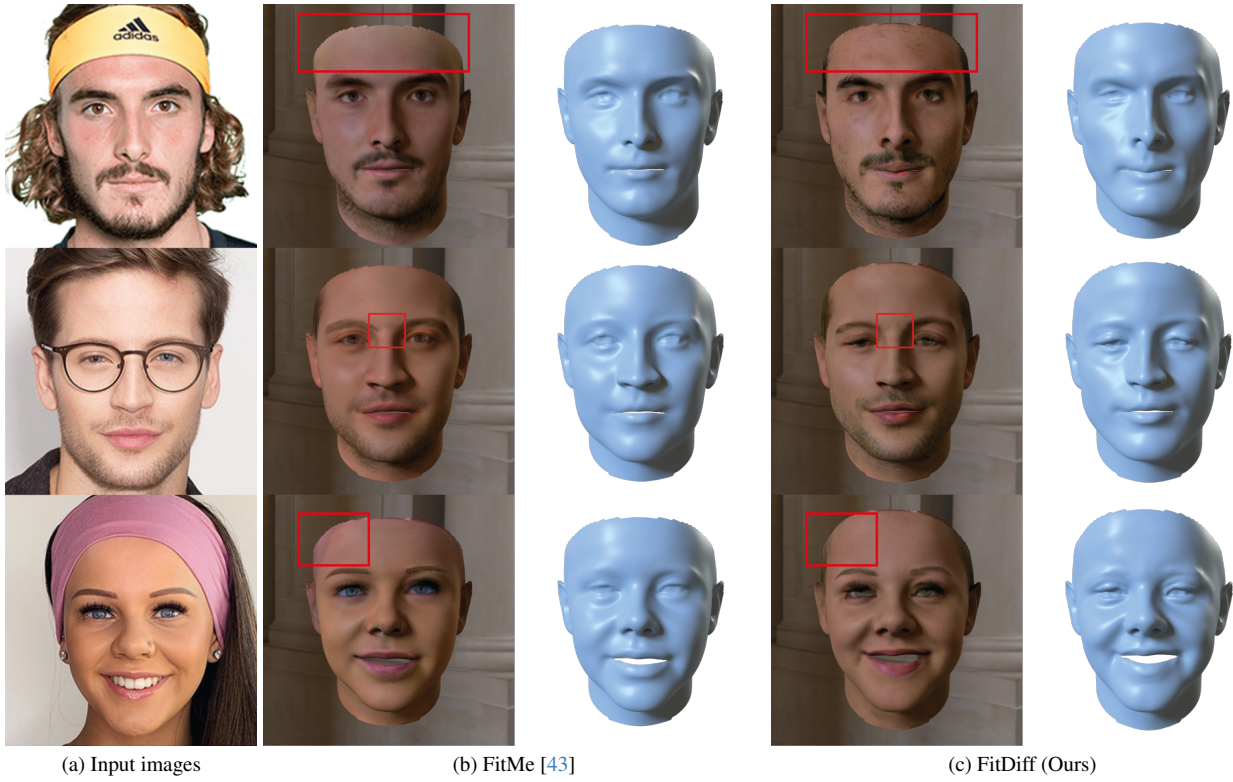


Figure 14. We examine our method’s samples in challenging images presented in FitMe [43]. FitMe’s reconstruction images were provided by the authors. Our reconstructions are not affected by any occlusions appearing in the input facial images.